IDE161, a potential first-in-class clinical candidate PARG inhibitor, selectively targets solid tumors with replication stress and DNA repair vulnerabilities

Diana Muñoz, Megan Conway, Pei Xin Lim, Vidhya Nagarajan, Arjun A. Rao, Ivan Shabalin, Kelly Trego, Jonathon Ryan, Rebeca M. Choy, Mason J. Appel, Zabrisky Roland, Peter Teriete, Richard Zang, Christian Frey, Yuchen Bai, Paul A. Barsanti, Claire Neilan, Mike White, Reeja Maskey

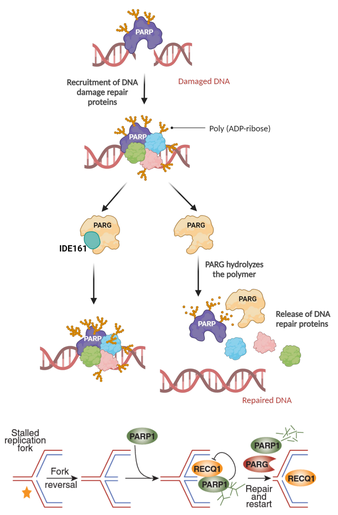
IDEAYA Biosciences, South San Francisco, CA USA

Summary

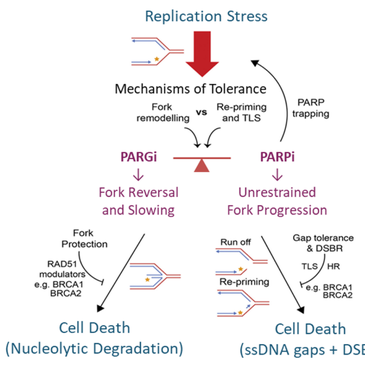
- Poly (ADP-Ribose) glycohydrolase (PARG), an enzyme involved in DNA damage response and DNA replication fork restart through hydrolysis of poly (ADP-ribose) (PAR) chains, has potential as an anti-cancer target in biomarker defined patient populations.
- IDE161 is a potent, orally bioavailable, small molecule that directly binds the active site of PARG to impede PAR chain hydrolysis.
- Evaluation of IDE161 antiproliferative activity across a panel of 350 molecularly characterized cancer cell lines highlighted significant associations of PARG-dependency with molecular signatures of chronic replication stress.
- Biomarker positive cancer cell lines responded to IDE161 exposure by activation of the ATR-mediated cell cycle checkpoint, and γ-H2AX signatures associated with pan-genomic replication fork collapse.
- Genome-wide CRISPR-mediated fitness screens across multiple genetic backgrounds revealed perturbation of gene products supporting DNA replication fork fidelity is sufficient to confer cellular vulnerability to IDE161.
- Consistent with genetic SL relationships, IDE161 induced single-strand gap accumulation, transcription-replication conflict (TRC), and extensive DNA replication fork progression defects in biomarker positive cancer cells.
- Notably, IDE161-dependent induction of TRC was associated with topoisomerase 1 cleavage complex accumulation, especially in combination with camptothecin, presumably due to accumulation of unresolvable DNA-protein conjugates (DPCs).
- Consistent with the DPC mechanism-of-action, IDE161 delivered exceptional anti-tumor activity in combination with fam-trastuzumab deruxtecan (Enhertu), an anti-HER2 ADC with a TOP1 inhibitor payload.
- These cumulative observations guide monotherapy patient selection strategies and indicate important combination opportunities.
- IDE161 is currently under evaluation in biomarker selected patients with advanced or metastatic cancers (NCT05787587).

Fig 1. PARG activity resolves PARP-initiated DNA repair complexes to support stalled replication fork stability and restart

A PARG hydrolyzes PAR chains to resolve DNA repair events

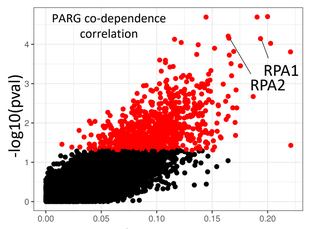


B PARG activity is selectively required for tolerance to replication stress

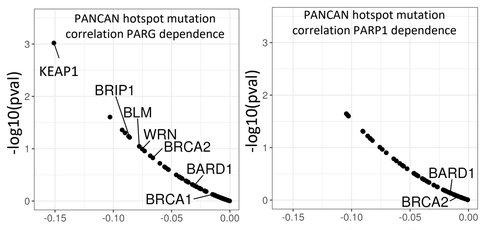


Schematics modified from Pillay et al., Progress in Biophysics and Molecular Biology 2021 and Pillay et al. Cancer Cell (2019)

C PARG shRNA co-dependency matrix highlights association with RSR genes



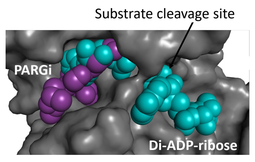
D PARG gene dependency is uniquely associated with mutations in RS genes compared to PARP1



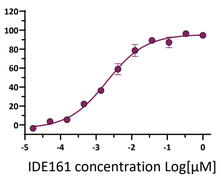
A) Schematic representation of **(Top)** the PARylation process and effect of PARG inhibition; **(Bottom)** stalled fork remodeling and stability **B)** Sensitivity to PARG versus PARP inhibitors. **C)** Project Achilles genome-scale co-dependency with PARG highlighting replication stress response hits among top correlates. Red points indicate p-value < 0.05. **D)** Correlation of hotspot mutations with PARG **(left)** and PARP1 **(right)** dependency. RNAi Data obtained from DepMap.

Fig 2. IDE161 is a potent, First-in-Class Phase 1 PARG inhibitor with highly selective target binding profile

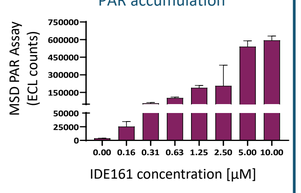
A X-ray co-crystal structure of IDE161



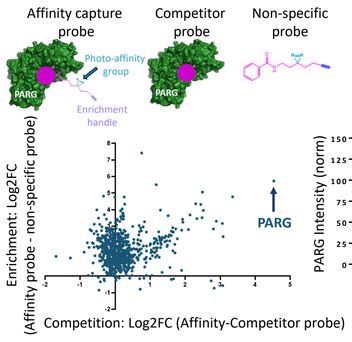
B IDE161 biochemical activity



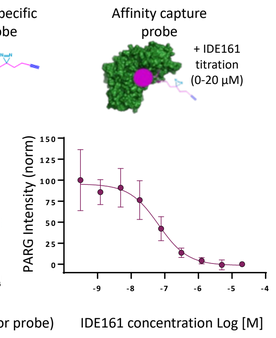
C IDE161-induced cellular PAR accumulation



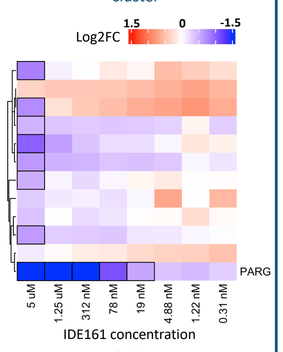
D High binding selectivity of IDE161-based affinity probe in the cellular proteome



E Significant IDE161 exposure-dependent target occupancy



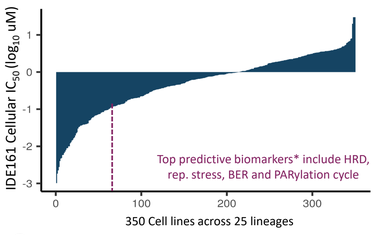
F Candidate IDE161-binders cluster



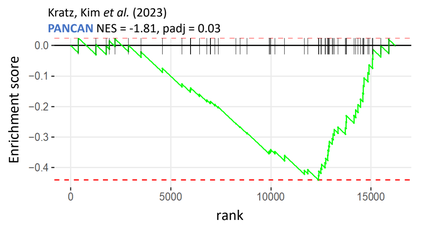
A) X-ray co-crystal structure of IDE161 (purple) bound to PARG (grey) and Di-ADP-ribose (cyan). **B)** Biochemical potency of IDE161 against human PARG. **C)** PAR chain accumulation assessed via MSD-based PAR assay in a gastric HRD line. **D)** Cellular target engagement assay schema and plot of distinct proteins selectively enriched from whole cell lysates using an IDE161-similar capture probe. **E)** Target occupancy determination and plot of PARG intensity after affinity capture in the presence of increasing concentrations of IDE161. **F)** Heatmap of log2FC of proteins tagged with capture probe in the presence of indicated IDE161 concentrations vs. DMSO control. Proteins with ≥ 0.9 Kendall correlation to PARG are depicted, and contrasts with Empirical Bayes moderated p-value < 0.05 are highlighted with a black box.

Fig 3. Response to IDE161 is associated with defects in DNA repair and chronic replication stress

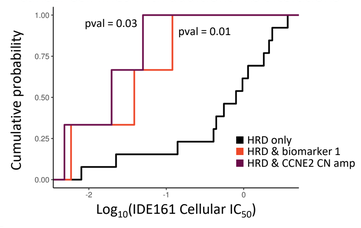
A IDC161 Cellular Viability Pan Cancer screen



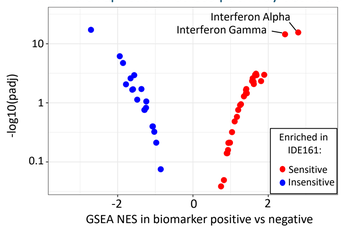
B Enrichment plot: DDRAM double stranded break Repair II



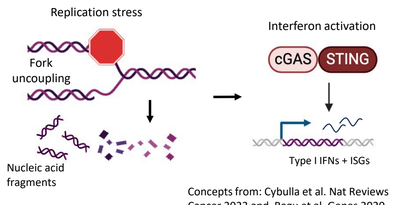
C Response to IDE161 is enriched in HRD ovarian cancer cell lines with additional RS alterations



D IDE161 response is associated with signatures of intrinsic replication stress pathway activation

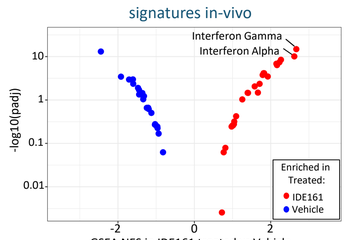


E Nucleic acid mediated interferon response is associated with replication stress



Concepts from: Cybulla et al. Nat Reviews Cancer 2023 and Ragu et al. Genes 2020

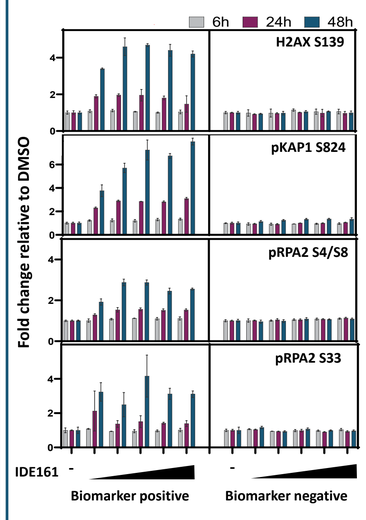
F IDE161 enhances tumor-associated interferon signatures in-vivo



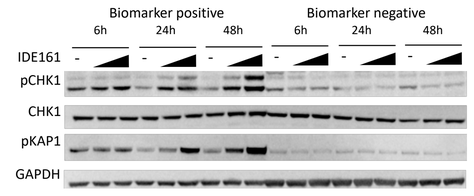
A) Waterfall plot of IDE161 IC_{50} values for 350 cell lines across 25 lineages representing a diversity of indications. *Models based on univariate and multivariate pan-cancer and lineage-specific molecular feature analysis. **B)** Enrichment plot of double stranded break repair from **D**NA **D**amage **R**esponse **A**ssemblies **M**ap (DDRAM) using baseline gene expression of IDE161 sensitive vs IDE161 insensitive cell lines; n=257 across 22 lineages**. C)** ECDF plot of IDE161 response in HRD OVCA cell lines with and without replication stress (RS); p-value from Kolmogorov–Smirnov test shown. HRD status obtained from Gulhan et. al (SigMA). **D)** GSEA volcano plot of MSigDB Hallmark gene sets in IDE161 sensitive vs. insensitive cell lines; IFN/STING pathway mediated gene expression signatures are labeled. **E)** Schematic indicating known relationship between RS and interferon response. **F)** GSEA volcano plot similar to (D) contrasting IDE161-treated ovarian CDX vs vehicle control at Day 37.

Fig 4. IDE161 selectively activates the replication stress and DNA damage response

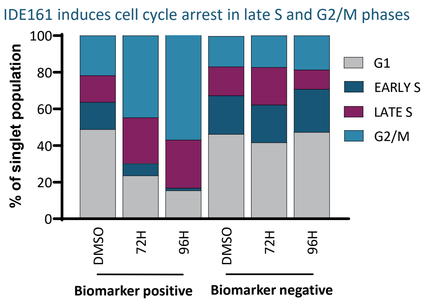
A IDE161 selectively induces DNA damage response markers



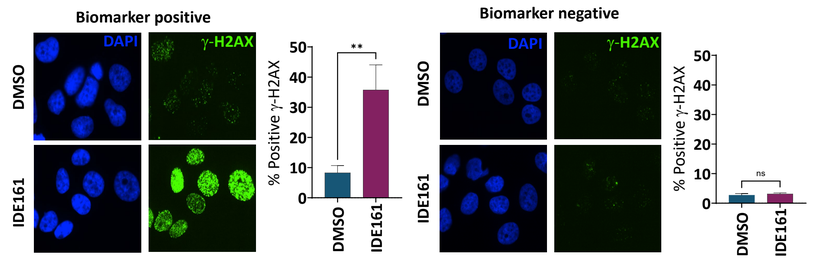
B IDE161 selectively activates ATM and ATR checkpoint signaling pathways



C IDE161 induces cell cycle arrest in late S and G2/M phases



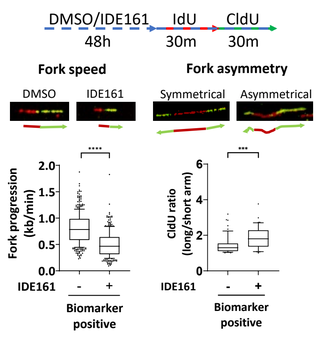
D IDE161 induces a γ-H2AX accumulation phenotype associated with replication catastrophe



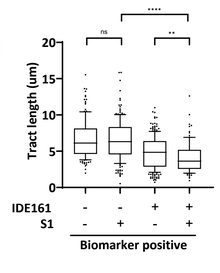
A) Accumulation of γ-H2AX, p-KAP1 and p-RPA was measured at indicated time using an MSD-based assay. Values are plotted as mean ± SD. **B)** Activation of pCHK1 and pKAP1 with IDE161 was evaluated by immunoblot blot. **C)** Cell cycle effects of IDE161 were evaluated by flow cytometry. **D)** Nuclear γ-H2AX was detected at 96 hours of IDE161 treatment using an anti- γ-H2AX antibody-based immunofluorescence assay. Quantitation of γ-H2AX staining is shown as % positive cells (mean ± SEM); positivity was defined by threshold at ~90th percentile mean intensity value in DMSO-treated biomarker positive cell line. Statistical analyses were performed using Student's t-test; ns (not significant), **(<0.01).

Fig 5. Cellular response to IDE161 is consistent with the role of PARG in maintaining replication fork fidelity in response to replication stress

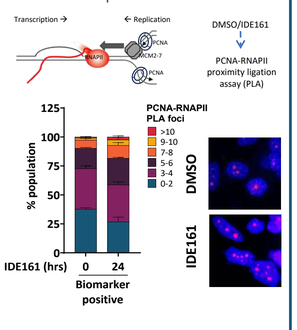
A IDE161 induces fork progression defects



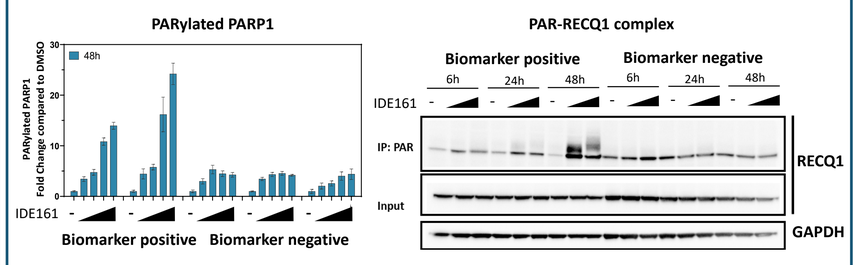
B IDE161 induces ssDNA gap accumulation



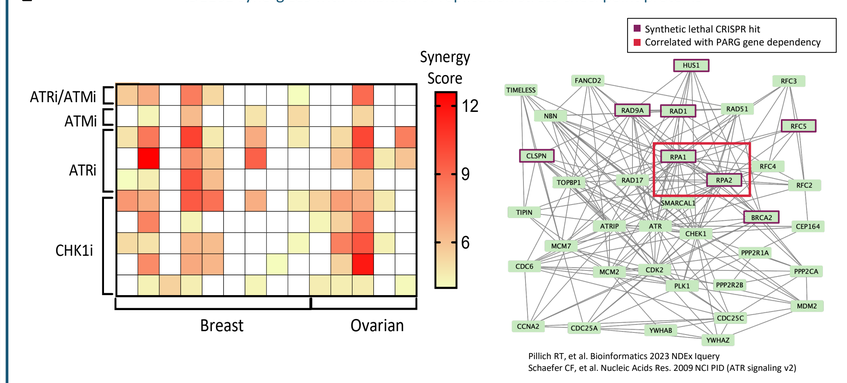
C IDE161 increases transcription-replication conflict



D IDE161 induces accumulation of PARylated PARP1 and stabilizes PAR-RECQ1 complex leading to replication arrest



E IDE161 synergizes with inhibition of replication stress checkpoint proteins

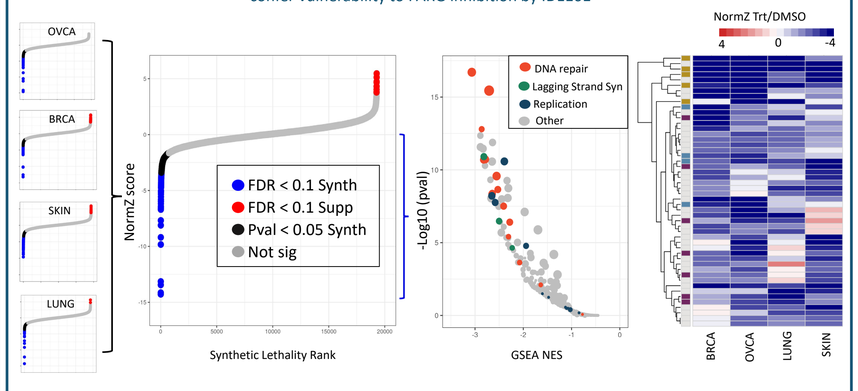


Pillich RT, et al. Bioinformatics 2023 NDEx Iquery
Schaefer CF, et al. Nucleic Acids Res. 2009 NCI PID (ATR signaling v2)

A) IDE161-mediated replication fork slowing **(Left)** and fork asymmetry **(Right)** as shown from measurements of CldU-labeled DNA fibers. Boxes indicate median and IQR. **B)** Accumulation of ssDNA gaps was evaluated via S1 nuclease DNA fiber assay. IdU labeled DNA fibers were measured from samples with indicated treatment. Boxes indicate median and IQR. Statistical analyses in **A)** and **B)** were performed using the Mann-Whitney U test; ns (not significant), **(<0.01), ***(<0.001), **** (<0.0001). **C)** Transcription-replication conflict was measured using a PCNA-RNAPII proximity ligation assay (PLA). PLA foci values were plotted as % population corresponding to the indicated range of PLA foci/cell. **D) (Left)** IDE161- mediated accumulation of PARylated PARP1 was measured at 48h using an MSD-based assay. Values are plotted as mean ± SEM. **(Right)** Accumulation of PARylated RECQ1 was measured using an anti-PAR immunoprecipitation (IP) assay. Input and IP samples were evaluated with anti-RECQ1 antibody by immunoblot. **E) (Left)** IDE161 was evaluated in combination with 90 drug partners in 14 cell lines in a 6x6 optimized dose matrix for 6 days. Heatmap indicates synergy scores, as assessed by the Loewe model, for inhibitor classes displaying significant synergy with IDE161. **(Right)** ATR checkpoint signaling interactome. Crimson boxes: Significant RSR-related PARG co-dependencies (Fig 1C). Purple boxes: Synthetic lethal hits in IDE161 CRISPR screen (Fig 6).

Fig 6. Functional genomic profiling reveals key IDE161 synthetic lethal relationships

A Perturbation of DNA repair, OFM/Lagging strand synthesis, or replication stress response is sufficient to confer vulnerability to PARG inhibition by IDE161



B Top 50 IDE161 synthetic lethal genes are enriched in mechanistic clusters supporting replication fork fidelity

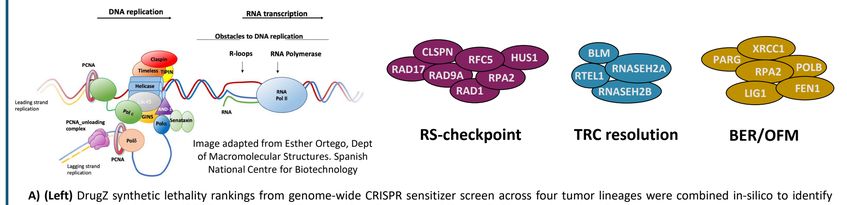
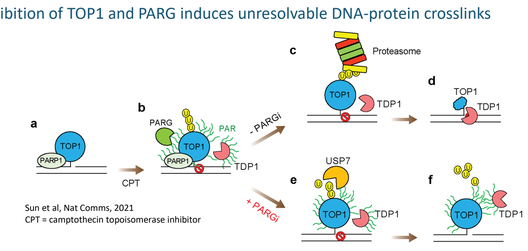


Image adapted from Esther Ortego, Dept of Macromolecular Structures. Spanish National Centre for Biotechnology

A) (Left) DrugZ synthetic lethality rankings from genome-wide CRISPR sensitizer screen across four tumor lineages were combined in-silico to identify tissue-agnostic sensitizers to IDE161 (at 2 doses: ~IC_{20} and ~IC_{40}; IC_{20} shown). **(Middle)** GSEA analysis of NormZ scores, from combined treated compared to combined DMSO samples, in REACTOME gene sets. Point size proportional to number of significantly differentially depleted genes in the leading edge. **(Right)** Heatmap of NormZ scores of top 50 synthetic lethal genes in low-dose IDE161 treated versus DMSO. Row annotations indicate functional enrichment of genes from relevant biological gene sets; RS-checkpoint (purple), TRC resolution (blue), and base excision repair/ Okazaki fragment maturation (BER/OFM; gold). **B) (Left)** Schematic depicting a functional replisome. **(Right)** Annotated membership of genes from aforementioned functional modules.

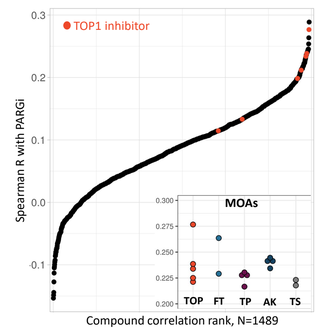
Fig 7. IDE161/TOP1 inhibitor combination exacerbates the accumulation of Topo1-DNA covalent complexes (TOP1cc) and PAR, leading to enhanced replication fork slowing and DNA damage

A Dual inhibition of TOP1 and PARG induces unresolvable DNA-protein crosslinks

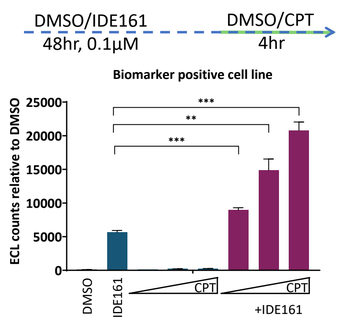


Sun et al, Nat Comms, 2021
CPT = camptothecin topoisomerase inhibitor

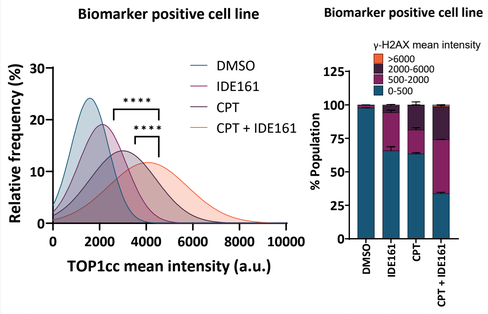
B PANCANCER drug assessments by PRISM indicates strong TOP1i/PARGi correlation



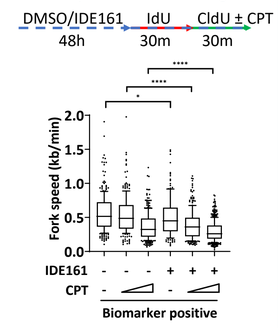
C TOP1i synergistically increases IDE161-mediated PAR accumulation in a dose dependent manner



D TOP1i/IDE161 combination leads to Top1cc accumulation and associated DNA damage



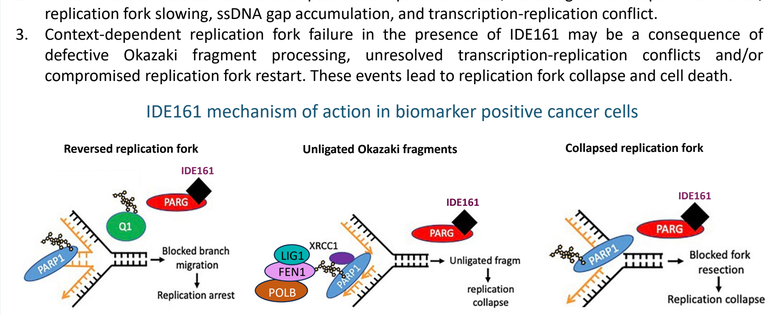
E TOP1i enhances IDE161-induced replication fork slowing



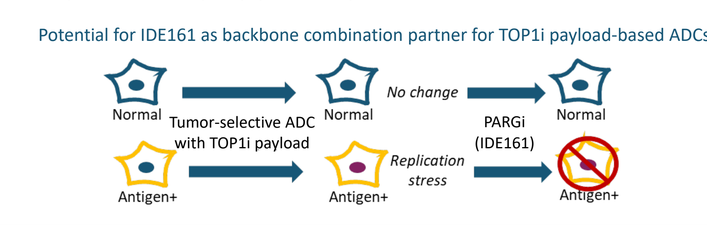
A) Model depicting proposed MOA for dual inhibition of TOP1 and PARG. **B)** Spearman correlation plot of response to PRISM compounds with PARGi; orange indicates TOP1 inhibitors, black indicates other. **(Inset)** Swarmplot of top correlated compounds grouped by MOA (MOAs with fewer than 2 compounds not shown). Topoisomerase inhibitor (TOP), farnesyltransferase (FT), tubulin polymerization (TP), aurora kinase (AK), thymidylate synthase (TS). **C)** PAR chain accumulation was evaluated using a PAR MSD assay. Values are plotted as mean ± SD relative to DMSO control. Statistical analyses were performed using Student's t-test; ns (not significant), **(<0.01), ***(<0.001). **D) (Left)** TOP1-DNA cleavage complexes (TOP1cc) were measured at indicated timepoint using anti-TOP1cc antibody-based immunofluorescence assay. Population binning and non-linear curve fit were performed based on TOP1cc mean intensity values in individual cells. Statistical analyses were performed using Kruskal-Wallis test; ****(<0.0001). **(Right)** Nuclear γ-H2AX was detected using anti- γ-H2AX antibody-based immunofluorescence assay. Values (mean ± SD) plotted as % population of γ-H2AX mean intensity ranges. **E)** Combined IDE161- and CPT-mediated replication fork slowing as shown from measurements of CldU-labeled DNA fibers. Boxes indicate median and IQR. Statistical analyses were performed using the Mann-Whitney U test; *(<0.05), **** (<0.0001).

Fig 8. Robust combination benefit with TOP1i payload-based ADC

A Combination of TOP1i-ADC and IDE161 delivers robust anti-tumor activity across lineages in CDX models



B The combination is well-tolerated preclinically leading to enhanced tumor PAR accumulation; further validating the persistence of unresolvable DNA-protein crosslinks

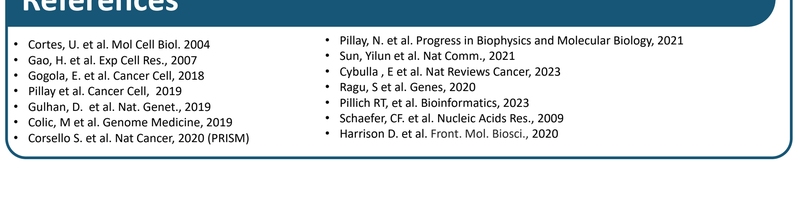


A) CDX combination efficacy across distinct lineages. Tumor growth curves represent the average response of 8 animals per group. Enhertu was administered intravenous as a single dose of 10 mg/kg and IDE161 was administered orally once or twice daily at 100mg/kg. HER2 annotation is based on NGS data **B)** PAR chain accumulation was evaluated using a PAR MSD assay after three days of dosing and body weight was measured twice weekly through the duration of the *in vivo* study.

Conclusions

1. Cellular vulnerability to PARG inhibition by IDE161 is associated with deficiencies in DNA repair and replication fork fidelity.
2. PARG inhibition induces hallmarks of persistent replication stress, including ATR checkpoint activation, replication fork slowing, ssDNA gap accumulation, and transcription-replication conflict.
3. Context-dependent replication fork failure in the presence of IDE161 may be a consequence of defective Okazaki fragment processing, unresolved transcription-replication conflicts and/or compromised replication fork restart. These events lead to replication fork collapse and cell death.

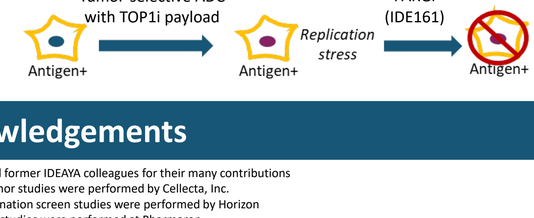
IDE161 mechanism of action in biomarker positive cancer cells



Adapted from Harrison D. et al. Frontiers 2020

4. IDE161 impairs resolution of TOP1 cleavage complexes (DNA/protein conjugates) to exacerbate TOP1i-induced DNA damage.
5. IDE161/TOP1i synergy can be exploited to enable efficacy for TOP1i-ADCs in models that otherwise fail to respond due to inadequate payload delivery.

Potential for IDE161 as backbone combination partner for TOP1i payload-based ADCs



Acknowledgements

- Present and former IDEAYA colleagues for their many contributions
- CRISPR anchor studies were performed by Cellecta, Inc.
- Drug combination screen studies were performed by Horizon
- *In vivo* CDX studies were performed at Pharmaron
- High content imaging from Molecular Devices

References

- Cortes, U. et al. Mol Cell Biol. 2004
- Gao, H. et al. Exp Cell Res., 2007
- Gogola, E. et al. Cancer Cell, 2018
- Pillay et al. Cancer Cell, 2019
- Gulhan, D. et al. Nat. Genet., 2019
- Colic, M et al. Genome Medicine, 2019
- Corsello S. et al. Nat Cancer, 2020 (PRISM)
- Pillay, N. et al. Progress in Biophysics and Molecular Biology, 2021
- Sun, Yilun et al. Nat Comm., 2021
- Cybulla , E et al. Nat Reviews Cancer, 2023
- Ragu, S et al. Genes, 2020
- Pillich RT, et al. Bioinformatics, 2023
- Schaefer, CF. et al. Nucleic Acids Res., 2009
- Harrison D. et al. Front. Mol. Biosci., 2020